IEEE Access
Multidisciplinary | Rapid Review | Open Access Journal

Received May 2, 2019, accepted May 22, 2019, date of publication May 31, 2019, date of current version June 19, 2019.

Digital Object Identifier 10.1109/ACCESS.2019.2920321

Influence of the Active Layer Material Quality and Doping Profile on the ZnO-Based MSM-PD's Performance

NAJEEB AL-KHALLI[1], MOHAMED ABOUD[2], AND NACER DEBBAR[1]
[1]Electrical Engineering Department, College of Engineering, King Saud University, Riyadh 11421, Saudi Arabia
[2]Sustainable Energy Technologies Center, College of Engineering, King Saud University, Riyadh 11421, Saudi Arabia

Corresponding author: Najeeb Al-Khalli (nageebalkhalli@gmail.com)

This work was supported in part by the Deanship of Scientific Research through the initiative of DSR Graduate Students Research Support (GSR).

ABSTRACT The active layer material quality and doping profile effects on the ZnO-based thin film metal-semiconductor-metal photodiode's (MSM-PD) performance are studied using a 2-D numerical simulation. The results of the simulation reveal that the temporal response advantages of increasing the doping concentration of the PD's active layer are only appreciable at low bias. Whereas, using the downgraded material, the temporal response advantages are maintained for all applied biases but at the expense of a very low responsivity. This paper discusses the possibility of improving the temporal response while maintaining excellent responsivity. It is shown that the composed structure, made of a good material heavily doped top layer and a bottom layer lightly doped made of downgrade material, exhibits the desired temporal response advantages while maintaining an excellent responsivity.

INDEX TERMS Metal-semiconductor-metal photodiode, numerical simulation, responsivity, temporal response, ZnO.

I. INTRODUCTION

Ultraviolet (UV) photodetectors based on Zinc-oxide (ZnO) thin film are in the attention of many researchers because of the material unique features. In contrast to other wide bandgap semiconductors, ZnO material possess higher resistance to high-energy particle irradiation, higher exciton binding energy, higher carriers saturation velocity, in addition to a simpler and lower cost fabrication process [1]–[3]. Many ZnO based photodetectors with different device structures have been reported in the literature [4]–[13]. As grown ZnO material is unintentionally n-type semiconductor; however obtaining stable and reproducible P-type ZnO material is still a very difficult process [3], [14], [15]. Therefore, the metal-semiconductor-metal (MSM) device structure has become the most attractive choice for photodiode (PD) applications [16], [17]. However, conventional ZnO-based MSM-PD suffers from low responsivity and response speed limitation [1]. MSM-PDs' response speed is primarily limited by the transit time of the photo-generated carriers [18], moreover, the transit time is governed by the mobility of the electrons and holes and the driving electric field established between the MSM-PD's fingers. The electric field depends on both the MSM-PD's structure (finger spacing and active layer thickness) and the applied bias. Because of their lower mobility, the holes are generally believed to cause the long tail in the temporal response; and thus, they represent the bottleneck of the PD speed. Consequently, the reduction or the complete elimination of the holes contribution to the photocurrent should definitely result in a significant improvement in photodiodes response time. A number of solutions have been proposed to improve the MSM-PDs speed. Mikulics et al, Chou et al, and R. B. Hammond et al, [19], [21] used active layer material with a very short lifetime to realize very high-speed MSM PDs. This downgraded material can be obtained by intentionally introducing high-density of recombination centers, impurities and/or defects, during the growth of the material. Currie and Chyi et al, [22], [23] used heterojunction to canalize the photo-generated carriers within a low bandgap and high mobility material. The skillfully crafted active layer caused the photo-generated carriers to drift towards the contacts in

The associate editor coordinating the review of this manuscript and approving it for publication was Kalyan Koley.

a predetermined path leading to very high response speed. Sun et al, [24] used a doped active layer to shorten the photodetector's fall time. Unfortunately, in all of these suggestions, the improvement of the response speed has been obtained at the expense of the responsivity of the MSM PDs, which is considerably lowered (sacrificed).

A number of theoretical [17], [25]–[30] and experimental [31]–[35] studies have also been reported that investigate the influence of the structure's parameters in an endeavor to improve the ZnO-based UV-PD performance. However, to the best of the author knowledge, no investigation has been carried out to study the active layer doping profile effects on the ZnO-based MSM-PD performance. This work presents an effort to study the effects of the doping profile on the responsivity and response time of MSM-PDs. The results are then employed in combination with previous suggestions in order to come up with an optimum design with improvement in the overall performances. In active layers with non-uniform doping concentration, the inter-region diffusion of majority carriers sets up a built-in electric field within the active layer normal to the surface of the structure. This internal electric field can have a significant impact on the charge carriers' dynamic (path) within the active layer which could be utilized to improve the UV-PD's performance.

In this paper, the performance of ZnO-based MSM-PDs with different doping profile and different material properties (i.e. carrier lifetime and mobility) are analyzed using a developed two-dimensional numerical simulation program. The model used is based on the drift-diffusion model; where the coupled system formed by the Poisson's equation and the time-dependent/time-independent continuity equations for electrons and holes is solved to evaluate the steady-state and transient response of the different MSM-PDs. The depletion region, electric field distributions, and current paths inside the MSM structures are considered in details to understand the carriers' dynamic behavior within the active layer of different doping profile MSM-PDs structures.

II. MODEL DESCRIPTION AND SIMULATED STRUCTURES

A schematic view of the studied ZnO- MSM-PD is shown in Fig.1 (a). The structure is composed of geometrically symmetrical interdigitated electrodes, which can be treated as a collocation of unit cells. These unit cells Fig.1 (b) are assumed to have the same physical properties; only one unit cell will be then considered as a simulation domain.

Poisson's equation and the time-dependent/time-independent continuity equations for electrons and holes represent the basic semiconductor equations based on the drift-diffusion model. These equations along with the appropriate boundary conditions are scaled, discretized, and solved using the finite difference approach on a non-uniform two-dimensional mesh, the details of the methodology employed to solve the system are presented in [29], [36], [37]. The ZnO material parameters utilized in the above-mentioned equations are shown in Table 1. Note the two values used for the mobility and lifetime.

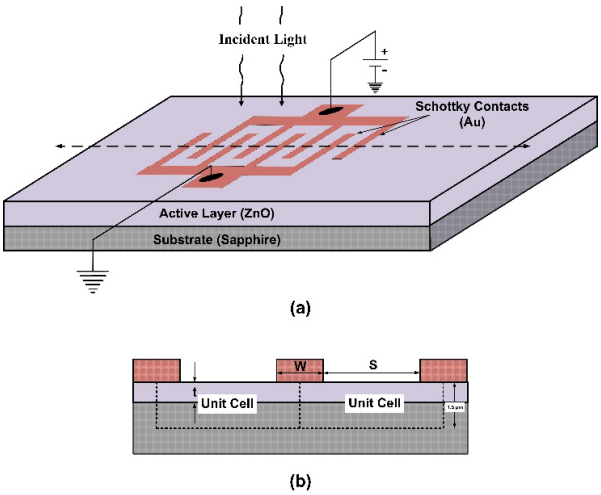

FIGURE 1. (a). Schematic view of the interdigitated MSM photodetector, (b) a cross-section of the simulated unit cell.

TABLE 1. ZnO thin film's parameters used for modeling.

Parameter	Symbol	Units	Values
Electron Mobility	μ_n	$cm^2/V.s$	250-50
Hole Mobility	μ_p	$cm^2/V.s$	50-10
Carrier lifetime	τ_n, τ_p	ps	250-5
Intrinsic carrier concentration	N_i	cm^{-3}	2.19E-11
Effective conduction band density of states	N_c	cm^{-3}	3.1E18
Effective valence band density of states	N_v	cm^{-3}	9.0E18
Relative permittivity	ε_s		8.5
Absorption coefficient	α	cm^{-1}	2.5e5
Band gap	E_g	eV	3.34
Wavelength	λ	nm	366
Refractive Index	n		2.014

The first numbers represent the typical values for the high-quality ZnO material, and the second represents the values for the downgraded materials. The low quality ZnO thin film can be fabricated using non optimal growth conditions such as substrate temperature, ambient gas, deposition pressure, and/or introducing high concentration of impurities [22].

Using the briefly described model above, a thorough investigation of the effect of modulation doped active layer on the performance of the ZnO-based MSM-PDs has been undertaken. The influence of the quality of the active layer material, which is symbolized by the values of the carrier's lifetime and mobility, is also considered in this comprehensive study. All analyzed MSM-PDs structures have $100 \times 100\ \mu m^2$ total active area and $0.2\ \mu m$ total active layer thickness. The optical illumination is assumed to be a uniform UV source incident from a top with $150\ \mu m$ spot diameter and $25\ \mu W$ UV optical power. To study the PDs' impulse response, a Gaussian optical signal is used with a full width at half maximum (FWHM) of $5\ ps$ and a peak located at $10\ ps$.

Several structures have been conceived to accomplish our study and realize an upmost understanding of the dynamics of photo-generated carriers in MSM-PDs. Our objective is

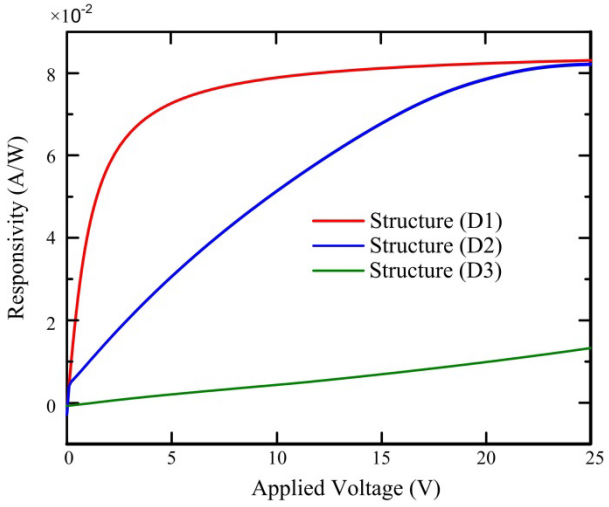

FIGURE 2. Calculated responsivity versus applied bias for MSM structures D1, D2, and D3 illuminated by 25 μW UV optical power.

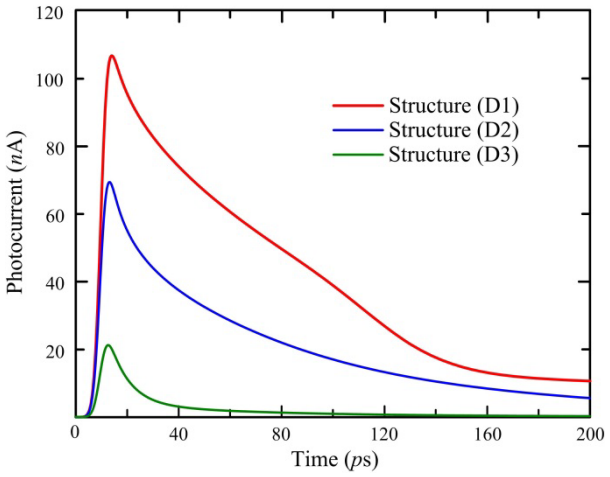

FIGURE 3. Calculated temporal response of MSM-PDs, structures D1, D2, and D3, at 5 V applied bias.

to arrive at the best MSM-PD design to achieve optimum performance. The structures have different active layer doping profiles and different material qualities. Our reference structure, denoted D1, is taken to have a uniform active layer ($N_D = 10^{15}$ cm^{-3} donor concentration unintentionally doped) with typical material quality. The second structure, denoted D2, has an n-doped active layer ($N_D = 10^{16}$ cm^{-3}) made also of typical material quality. The third structure, denoted D3, has an un-doped uniform active layer ($N_D = 10^{15}$ cm^{-3}) constituted from intentionally downgraded material quality. The fourth structure, denoted D4, has an active layer composed of two regions of typical material quality but different dopings: a 0.1 μm n-doped ($N_D = 10^{16}$ cm^{-3}) top layer and a 0.1 μm un-doped ($N_D = 10^{15}$ cm^{-3}) layer underneath. The fifth structure denoted D5, is composed of two layers: a 0.1 μm top layer of normal material quality n-doped ($N_D = 10^{16}$ cm^{-3}) and a 0.1 μm bottom layer un-doped ($N_D = 10^{15}$ cm^{-3}) downgraded material quality. It should be noted that the downgraded material can be formed by growing the material under non optimum condition leading to high concentration of defects; and/or introducing a large concentration of impurities. The carriers in the downgraded material usually have much lower mobility and much shorter lifetime Table 1 [22].

III. SIMULATION RESULTS AND DISCUSSION

As mentioned in the introduction, a doped active layer as well as a downgraded active layer material with a very short recombination lifetime were proposed to speed up the MSM-PDs' response. Therefore, the study started by investigating the impact of these two modifications, structures D2 and D3, on the responsivity and response speed and compares them with the reference structure D1. Figure 2 shows the responsivity versus applied bias of the three structures under dc illumination. It can be seen that increasing the doping concentration of the PD's active layer (structure D2) delays the saturation of the responsivity up to higher applied biases. The saturation usually occurs when the active layer becomes fully depleted and hence most of the photo-generated carriers are collected. Since the extent of the depletion region depends considerably on the doping concentration; the highly doped structure (D2) necessitates higher applied bias to reach the saturation. Thus, the difference on the responsivity between D1 and D2 decreases with increasing the bias and both devices responsivity tend to saturate around 0.082 A/W. On the other hand structure D3, made with the downgraded material, yields a very low responsivity over the whole range of applied bias due to the high recombination rate caused by the very short lifetime of excess carriers. It must be noted that the extent of the depletion region and the electric field distribution, strength and direction, within the active layer of structure D3 and structure D1 are nearly identical; and both structures require around 5 volt bias to fully deplete the active layer.

Figure 3 shows the calculated impulse response for structures D1, D2, and D3 at an applied bias of 5 volts. It can be seen that all devices exhibit nearly identical rise time around 4.5 *ps* that tracks very closely the excitation impulse (FWHM = 5 *ps*). On the other hand, they reveal significant differences in the peak photocurrent, FWHM, and fall time. These differences are believed to be correlated to the dissimilarity in the expansion of the depletion region in the active layer because of the high doping for structure D2 and the elevated recombination rate of the photo-generated carriers caused by the short lifetime for structure D3. The main advantages of the proposed structures D2 and D3 over the reference structure D1 are the shorter FWHM and fall time in the impulse response; resulting in a much faster response time of the devices. For structure D2 these advantages, when compared to D1, are only appreciable at low bias whereas as the applied bias is increased the two structures exhibit comparable response speed Fig. 11 and 12.

These observations can be easily explained by carefully examining the evolution of the depletion region for the two

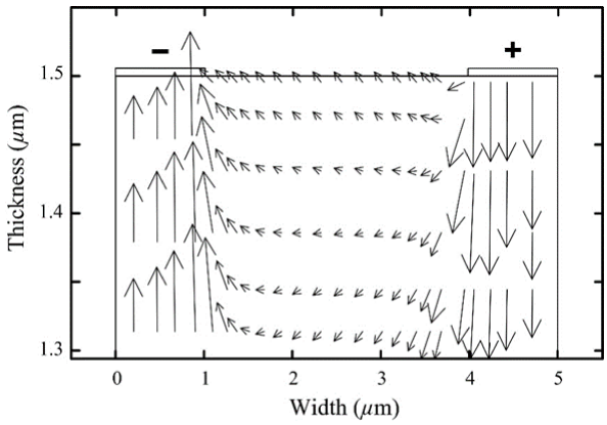

FIGURE 4. Vector plot of the electrical field distribution within the active layer of structure D1 at 15 V applied bias.

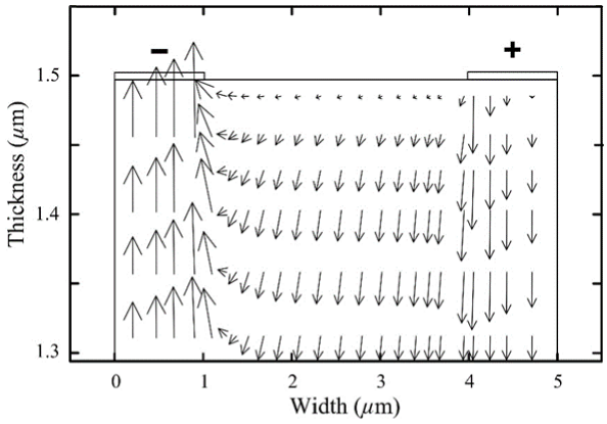

FIGURE 5. Vector plot of the electrical field distribution within the active layer of structure D4 at 15 V applied bias.

structures. The extent of the depletion region at a given bias is smaller for structure D2 because of the higher doping; therefore, the collection of photo generated carriers covering mainly the depleted region completes faster. However, as the bias is increased and the depletion region extends over the whole active layer these advantages gradually disappear. Concerning structure D3, made from the downgraded material, the advantages of the temporal response are maintained for all applied biases. However, the dc responsivity and the peak photocurrent of the impulse response are extremely lower than all other structures. This structure can be very useful in special applications where the incident optical signal is appreciable and the response speed is the main objective of the system.

In an effort to devise structures with even superior performances than the structures proposed in the literature and studied above. The authors considered ways to reduce the contribution of the slow holes in the overall photocurrent; as they are generally thought to be the cause of the long tail in the impulse response. Thus, the device can achieve a much faster response time while keeping acceptable responsivity. It is well known that the electric field distribution in the PD's active layer determines its photo-response [38]. Therefore, a study of the doping profile impact on the PD's responsivity and response speed started by investigating the electric field distribution, direction and strength, within the active layer of the device. The effects caused by changing the active layer doping profile on this distribution were careful examined. The structure D4 has been selected to establish the conditions under which the photo-generated electrons and hole will have the desired drift paths within the active layer. The built-in electric field established by the non-uniform doping should have the required direction to repel the photo-generated holes away from the top region. Therefore, the device structure could result in hindering the slow holes from being collected leading to substantially shortening the long tail in the temporal response.

The simulation under dark condition is carried out for structures D1 and D4 at an applied bias of 15 V. Figures 4, and 5 show the calculated electric field distribution in vector forms, strength and direction, in the active layer for D1 and D4, respectively. Because the electric fields in the vicinity of the contacts are much stronger compared to those in the central region of the active layer, the vectors shown in the figures were scaled down differently for the two regions. Thus, the figures exhibit accurately the directions of the electric field within the devices and relatively their strength. Careful examination of the electric fields distributions in the two figures reveals a number of features that could have profound impacts on the paths followed by the drifting photo generated carriers. In structure D1, uniform doping, between the contacts the electric field is nearly uniform principally pointing in the negative x-direction.

Whereas, in structure D4, non-uniform doping, the field distribution between the contacts is modified fundamentally; the electric fields are mostly pointing downward. The negative y-components of the fields have increased in strength by about three orders of magnitude compared to those in structure D1, while the x-components remain approximately the same. This transformation is the most important; it could be utilized ingeniously in MSM-PD designs to reduce the long tail in the temporal response or eliminate it altogether. The intense y-components of the electric field, set up because of the non-uniform doping, repel the photo-generated holes away from the active layer toward the substrate and hence prevent their contribution to the photocurrent. Structure D4 is then simulated to evaluate its performance under dc illumination and impulse optical signal. The dc responsivity obtained have very similar trend like structure D1 and structure D2: the responsivity increases monotonically with applied bias until reaching a saturation value of about 0.082 A/W. Even though, because of the difference in doping concentration/profile between the three structures the saturation is attained at different applied bias. Unfortunately, the response time has not improved and even deteriorated at certain applied biases. The problem with the structure is it drives the holes downwards, and since the carriers' lifetime is too long the photo-generated holes finish by being collected but inopportunely after following a longer

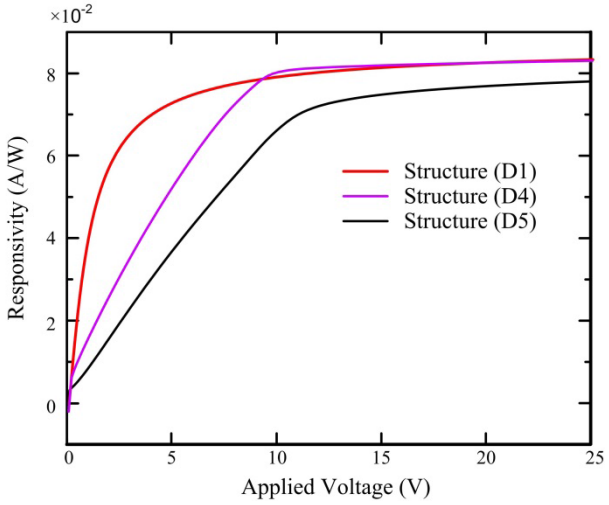

FIGURE 6. Calculated responsivity versus applied bias for MSM structures D1, D4, and D5 illuminated by 25 μW UV optical power.

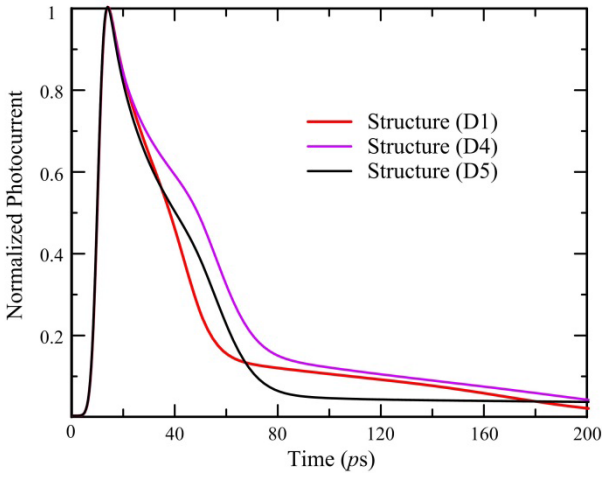

FIGURE 7. Normalized temporal responses of MSM-PDs, structures D1, D4, and D5, at 15 V applied bias.

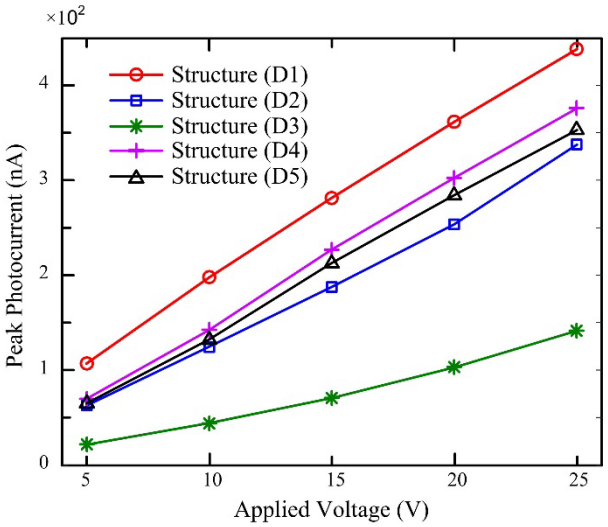

FIGURE 8. Peak photocurrent versus applied bias for the different MSM-PDs structures.

path. Video 1 shows the photo-generated electrons and holes behavior within the active layer of structure D4 as a response of the Gaussian optical signal at bias 15 volt.

Consequently, we should annihilate the repelled holes to prevent their contribution to the photocurrent; hence the repelling of the holes could materialize in improvement of response speed. Structure D5 is devised to take advantage of the two ideas: (1) the repelling of the holes by the non-uniform doping; and (2) the shortening of the carriers' lifetime by using downgraded material in the bottom layer. As described above, structure D5 is composed of a top layer made of good material heavily doped, and a bottom layer lightly doped made of downgrade material.

Figure 6 shows the dc responsivity versus applied bias for structures D1, D4, and D5. The proposed structure D5 shows a very slight degradation in dc responsivity: saturation at $\sim$ 0.077 A/W compared to 0.082 A/W of the reference structure D1. Figure 7 shows the normalized impulse response of the three structures at 15 V applied bias. Even though, the FWHM is comparable between the three structures at this bias the figure reveals very clearly the improvement in the fall time of the proposed structure. This is a strong indication that the holes repelled toward the bottom layer are hindered from contributing to the photocurrent. The obstruction could be caused by either of two factors. One the elevated recombination rate in the bottom downgraded layer results in the annihilation of these holes. Two the very low mobility within this layer hampers these holes from drifting back towards the contacts to become collected

Figures 8, 9 and 10 summarize the calculated peak photocurrent, FWHM and fall time versus applied bias for all simulated structures; these three figures of merit are directly related to the performance of photodetectors.

The figures reveal a strong bias dependence of these performance parameters. As the bias is increased and the active layer becomes fully depleted, all structures manifest a monotonically increase of the peak photocurrent, and decrease in the fall time. The FWHM for all structures tends to saturate for high biases at a very comparable value except for structure D3, made of the downgraded material, it maintains a noticeably smaller FWHM for all bias range. The fluctuation in the fall time of the curves D4 and D5 seen in Fig. 10 around 10 V, is believed to be correlated to the spreading of the depletion region across the two region of different doping.

The proposed structure, D5, exhibits a clear superiority in the fall time, comparable to structure D3 made of the downgraded material while maintaining an excellent responsivity comparable to that achieved by structure D1. The proposed structure offers a much superior design for MSM PD applications; it exhibits a significantly faster response time without severely sacrificing the responsivity.

Further fine adjustments may be required to further improve the performance of the structure. Adjustments of

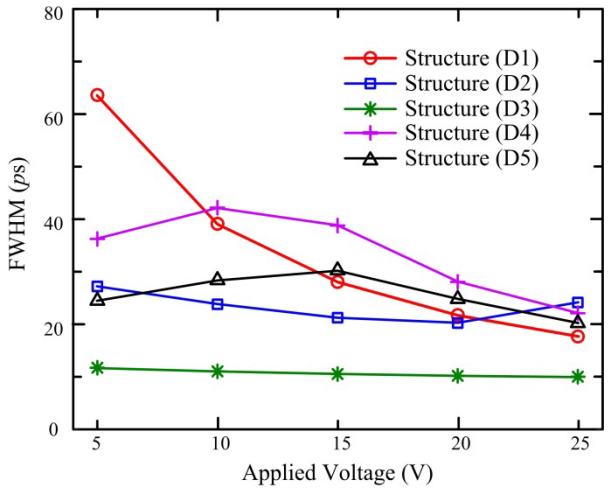

FIGURE 9. FWHM time versus applied bias for the different MSM-PDs structures.

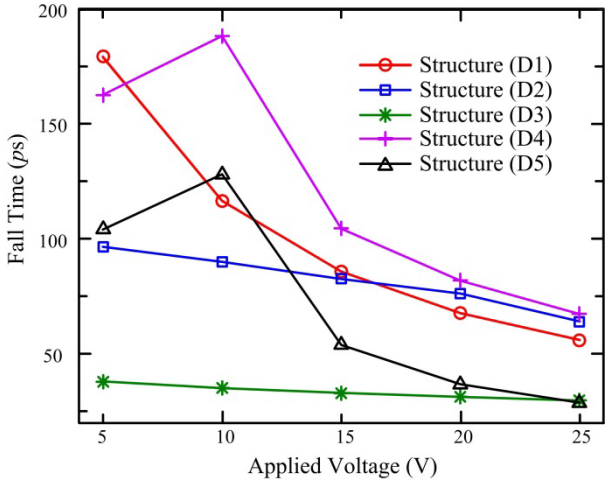

FIGURE 10. Fall time versus applied bias for the different MSM-PDs structures.

the thickness and doping concentrations of the top and bottom layers could lead to further optimization of the PD performance.

IV. CONCLUSION

The DC and temporal response of ZnO-based MSM-PDs, where the active layer has different doping concentration/profile and made of different material quality, are analyzed using a two-dimensional numerical simulation program. The results of the simulation show that increasing the doping concentration of the active layer lead to an improvement of the response speed. Unfortunately, this advantage is only appreciable at low bias when the depletion region is relatively smaller because of the high doping concentration. At high bias when the whole active layer becomes fully depleted the advantage disappear. On the other hand, using an active layer made of downgraded ZnO material result in an MSM-PD with excellent response time over the whole bias range. Yet again this advantage is obtained at the expense of the responsivity. Conscientious examinations of the electric field distribution and the dynamics of the photo-generated carriers lead to the conception of a new design for the MSM PD. The new design consists of an active region made of two layers; the top layer a heavily doped n-type good quality ZnO material, and the bottom layer a lightly doped n-type downgraded ZnO material. The main advantage of the new design is to ingeniously drive the slow hole away from the active layer, and preclude their contribution to the photocurrent. The simulation results of the devised structure show a much faster response time with very short fall time. In addition, the responsivity of the MSM-PD structure shows no significant degradation. The new structure exhibited superior overall performance over all previously suggested designs.

REFERENCES

[1] K. Liu, M. Sakurai, and M. Aono, "ZnO-based ultraviolet photodetectors," *Sensors*, vol. 10, no. 9, pp. 8604–8634, 2010.
[2] V. A. Coleman and C. Jagadish, "Basic properties and applications of ZnO," in *Zinc Oxide Bulk, Thin Films and Nanostructures: Processing, Properties, and Applications*, Amsterdam, The Netherlands: Elsevier, 2006, ch. 1, pp. 1–20.
[3] Z. Alaie, S. M. Nejad, and M. H. Yousefi, "Recent advances in ultraviolet photodetectors," *Mater. Sci. Semicond. Process.*, vol. 29, pp. 16–55, Jan. 2015.
[4] T.-H. Moon, M.-C. Jeong, W. Lee, and J.-M. Myoung, "The fabrication and characterization of ZnO UV detector," *Appl. Surf. Sci.*, vol. 240, pp. 280–285, Feb. 2005.
[5] Y. R. Ryu, T. S. Lee, J. A. Lubguban, H. W. White, Y. S. Park, and C. J. Youn, "ZnO devices: Photodiodes and *p*-type field-effect transistors," *Appl. Phys. Lett.*, vol. 87, no. 15, 2005, Art. no. 153504.
[6] O. Lopatiuk-Tirpak, L. Chernyak, L. J. Mandalapu, Z. Yang, J. L. Liu, K. Gartsman, Y. Feldman, and Z. Dashevsky, "Influence of electron injection on the photoresponse of ZnO homojunction diodes," *Appl. Phys. Lett.*, vol. 89, no. 14, 2006, Art. no. 142114.
[7] T.-S. Lin and C.-T. Lee, "Performance investigation of pin ZnO-based thin film homojunction ultraviolet photodetectors," *Appl. Phys. Lett.*, vol. 101, no. 22, 2012, Art. no. 221118.
[8] K. Wang, Y. Vygranenko, and A. Nathan, "Optically transparent ZnO-based n-i-p ultraviolet photodetectors," *Thin Solid Films*, vol. 515, pp. 6981–6985, Jun. 2007.
[9] J. D. Hwang, D. H. Wu, and S. B. Hwang, "Inserting an i-ZnO layer to increase the performance of p-Si/n-ZnO heterojunction photodetectors," *Mater. Sci. Semicond. Process.*, vol. 39, pp. 132–135, Nov. 2015.
[10] S. Liang, H. Sheng, Y. Liu, Z. Huo, Y. Lu, and H. Shen, "ZnO Schottky ultraviolet photodetectors," *J. Cryst. Growth*, vol. 225, nos. 2–4, pp. 110–113, May 2001.
[11] S. Singh and S.-H. Park, "Fabrication and characterization of Al:ZnO based MSM ultraviolet photodetectors," *Superlattices Microstruct.*, vol. 86, pp. 412–417, Oct. 2015.
[12] M. A. Ghusoon and P. Chakrabarti, "ZnO-based interdigitated MSM and MISIM ultraviolet photodetectors," *J. Phys. D, Appl. Phys.*, vol. 43, no. 41, 2010, Art. no. 415103.
[13] T. Zhang, J. Yu, Y. F. Deng, N. Tian, and P. Gao, "Fast response ultraviolet photodetectors based on solution-processed ZnO nanocrystals," *Sci. China Technol. Sci.*, vol. 58, pp. 1328–1332, Aug. 2015.
[14] D. C. Look, "Doping and Defects in ZnO," in *Zinc Oxide Bulk, Thin Films and Nanostructures: Processing, Properties, and Applications*. Amsterdam, The Netherlands: Elsevier, 2006, ch. 2, pp. 21–42.
[15] Y. Hou, Z. Mei, and X. Du, "Semiconductor ultraviolet photodetectors based on ZnO and $Mg_xZn_{1-x}O$," *J. Phys. D, Appl. Phys.*, vol. 47, Jun. 2014, Art. no. 283001.
[16] D. Çalişkan, B. Bütün, M. C. Çakir, S. Özcan, and E. Özbay, "Low dark current and high speed ZnO metal-semiconductor-metal photodetector on SiO_2/Si substrate," *Appl. Phys. Lett.*, vol. 105, Oct. 2014, Art. no. 161108.
[17] P. Wang, Z. Song, J. He, X. Guo, Y. Wang, L. Qiu, L. Guo, and Y. Yang, "Effects of internal gain and illumination-induced stored charges in MgZnO metal-semiconductor-metal photodetectors," *IEEE Trans. Electron Devices*, vol. 63, no. 4, pp. 1600–1607, Apr. 2016.

[18] P. R. Berger, "Metal-semiconductor-metal photodetectors," *Proc. SPIE*, vol. 4285, pp. 198–208, May 2001.
[19] M. Mikulics, M. Marso, P. Javorka, P. Kordoš, H. Lüth, M. Kočan, A. Rizzi, S. Wu, and R. Sobolewski, "Ultrafast metal-semiconductor-metal photodetectors on low-temperature-grown GaN," *Appl. Phys. Lett.*, vol. 86, Apr. 2005, Art. no. 211110.
[20] S. Y. Chou and M. Y. Liu, "Nanoscale tera-hertz metal-semiconductor-metal photodetectors," *IEEE J. Quantum Electron.*, vol. 28, no. 10, pp. 2358–2368, Oct. 1992.
[21] R. B. Hammond, N. G. Paulter, R. S. Wagner, and T. E. Springer, "Excitation and Fe concentration dependences in the impulse photoconductance of InP:Fe," *Appl. Phys. Lett.*, vol. 44, no. 6, pp. 620–622, 1984.
[22] M. Currie, "Low-temperature grown gallium arsenide (LT-GaAs) high-speed detectors," in *Photodetectors: Materials, Devices and Applications*, B. Nabet, Ed. Cambridge, U.K: Woodhead Publishing, 2016, pp. 121–155.
[23] J.-I. Chyi, Y.-J. Chien, R.-H. Yuang, J.-L. Shieh, J.-W. Pan, and J.-S. Chen, "Reduction of hole transit time in GaAs MSM photodetectors by p-type/spl delta/-doping," *IEEE Photon. Technol. Lett.*, vol. 8, no. 11, pp. 1525–1527, Nov. 1996.
[24] J. Sun, F.-J. Liu, H.-Q. Huang, J.-W. Zhao, Z.-F. Hu, X.-Q. Zhang, and Y.-S. Wang, "Fast response ultraviolet photoconductive detectors based on Ga-doped ZnO films grown by radio-frequency magnetron sputtering," *Appl. Surf. Sci.*, vol. 257, pp. 921–924, Nov. 2010.
[25] P. Wang, Q. Zhen, Q. Tang, Y. Yang, L. Guo, K. Ding, and F. Huang, "Steady-state characteristics and transient response of MgZnO-based metal-semiconductor-metal solar-blind ultraviolet photodetector with three types of electrode structures," *Opt. Express*, vol. 21, no. 15, pp. 18387–18397, Jul. 2013.
[26] S. Singh, "Simulation, fabrication, and characterization of Al-doped ZnO-based ultraviolet photodetectors," *J. Electron. Mater.*, vol. 45, pp. 535–540, Jan. 2016.
[27] G. Harzallah and M. Remram, "Ultraviolet MSM photodetector with fast response based on ZnO thin film," *Int. J. Nanoparticles*, vol. 6, nos2–3, pp. 153–160, 2013.
[28] S. Sharma, A. Sumathi, and C. Periasamy, "Photodetection properties of ZnO/Si heterojunction diode: A simulation study," *IETE Tech. Rev.*, vol. 34, pp. 83–90, Feb. 2016.
[29] N. Al-Khalli and N. Debbar, "Performance enhancement of ZnO-based MSM photodiodes by optimizing structure parameters," *Int. J. Numer. Model., Electron. Netw. Devices Fields*, vol. 32, no. 2, p. e2519, 2019.
[30] A. El-Amin, "High efficiency computer simulation for Au/n-ZnO/p-Si/Al Schottky-type thin film heterojunctions," *Silicon*, vol. 9, no. 3, pp. 385–393, 2016.
[31] J.-D. Hwang, G.-S. Lin, and S.-B. Hwang, "Effects of $Mg_xZn_{1-x}O$ thickness on the bandwidth of metal-semiconductor-metal bandpass photodetectors," *IEEE Trans. Electron Devices*, vol. 64, no. 1, pp. 195–199, Jan. 2017.
[32] Q. Zheng, F. Huang, K. Ding, J. Huang, D. Chen, Z. Zhan, and Z. Lin, "MgZnO-based metal-semiconductor-metal solar-blind photodetectors on ZnO substrates," *Appl. Phys. Lett.*, vol. 98, no. 22, p. 221112, Jun. 2011.
[33] K. Wang, F. Chen, N. Allec, and K. S. Karim, "Fast lateral amorphous-selenium metal-semiconductor-metal photodetector with high blue-to-ultraviolet responsivity," *IEEE Trans. Electron Devices*, vol. 57, no. 8, pp. 1953–1958, Aug. 2010.
[34] H.-Y. Lee, Y.-T. Hsu, and C.-T. Lee, "ZnO-based resonant cavity enhanced metal-semiconductor-metal ultraviolet photodetectors," *Solid-State Electron.*, vol. 79, pp. 223–226, Jan. 2013.
[35] H.-Y. Chen, K.-W. Liu, X. Chen, Z.-Z. Zhang, M.-M. Fan, M.-M. Jiang, X.-H. Xie, H.-F. Zhao, and D.-Z. Shen, "Realization of a self-powered ZnO MSM UV photodetector with high responsivity using an asymmetric pair of Au electrodes," *J. Mater. Chem. C*, vol. 2, no. 45, pp. 9689–9694, 2014.
[36] N. Debbar, "Investigation of the dark electrical characteristics of the lateral metal-semiconductor-metal photodetectors using two-dimensional numerical simulation," *Int. J. Numer. Model. Electron. Netw. Devices Fields*, vol. 24, pp. 335–344, Jul./Aug. 2011.
[37] N. Debbar, "Theoretical study of the DC and transient characteristics of a lateral Schottky barrier photodiode for application as high-speed photodetector," *Int. J. Numer. Model. Electron. Netw. Devices Fields*, vol. 29, pp. 333–342, Mar./Apr. 2016.
[38] J. B. D. Soole and H. Schumacher, "InGaAs metal-semiconductor-metal photodetectors for long wavelength optical communications," *IEEE J. Quantum Electron.*, vol. 27, no. 3, pp. 737–752, Mar. 1991.

NAJEEB AL-KHALLI received the B.Sc. degree in biomedical engineering from Hashemite University, Zarqa, Jordan, in 2007, and the M.S. degree in electronic from King Saud University (KSU), Riyadh, Saudi Arabia, in 2013, where he is currently pursuing the Ph.D. degree in electronic. From 2010 to 2014, he was a Research Assistant with Prince Sultan Advanced Technology Research Institute (PSATRI). Since 2014, he has been a Researcher with the Electrical Engineering Department, KSU. His research interest includes photodiodes and microbolometer designing and fabrication.

MOHAMED ABOUD received the B.Sc. degree in metallurgical engineering from Cairo University, Egypt, in 1992, the M.S. degree in materials engineering from Drexel University, Philadelphia, PA, USA, in1999, and the Ph.D. degree in materials engineering from Temple University, Philadelphia, in 2006. He was appointed as Adjunct Professor with Temple University for one year. He was an Assistant Professor with the College of Engineering, Al-Azhar University, from 2007 to 2010. He joined King Saud University, as an Assistant Professor, in 2010. His current research interests include fabrications of nano-materials and thin films using wet chemical methods, and evaporation techniques for renewable energy applications.

NACER DEBBAR received the D.E.S. degree in physics from the University of Constantine, Algeria, in 1982, and the M.S. degree in electrical science and the Ph.D. degree in electrical engineering from the University of Michigan, Ann Arbor, in 1984 and 1989, respectively. From 1990 to 1992, he conducted postdoctoral studies in the area of high-speed optoelectronic devices and optoelectronic integration with the EPFL, Lausanne, Switzerland. For one year, he was a Visiting Postdoctorate with Bilkent University, Ankara, Turkey. From 1993 to 1995, he was an Assistant Professor with the Physics Department, United Arab Emirates University. In 1995, he joined King Saud University, Saudi Arabia, as an Assistant Professor in electrical engineering, and has been a Professor, since 2017. His current research interest includes modeling and simulation of semiconductor devices, especially GaAs-based and ZnO-based devices and heterostructures.